Acceleration of global N_2O emissions seen from two decades of atmospheric inversion

R. L. Thompson[1]*, L. Lassaletta[2], P. K. Patra[3], C. Wilson[4,5], K. C. Wells[6], A. Gressent[7],
E. N. Koffi[8], M. P. Chipperfield[4,5], W. Winiwarter[9,10], E. A. Davidson[11], H. Tian[12]
and J. G. Canadell[13].

1. Norsk Institutt for Luftforskning (NILU), Kjeller, Norway
2. CEIGRAM-Agricultural Production, Universidad Politécnica de Madrid, Madrid, Spain
3. Research Institute for Global Change, JAMSTEC, Yokohama 236 0001, Japan
4. National Centre for Earth Observation, University of Leeds, Leeds, UK
5. School of Earth and Environment, University of Leeds, Leeds, UK
6. Department of Soil, Water, and Climate, University of Minnesota, MN, USA
7. Massachusetts Institute of Technology, Cambridge, MA, USA
8. European Commission Joint Research Centre, Ispra, Italy
9. IIASA, Laxenburg, Austria
10. University of Zielona Góra, Poland
11. University of Maryland Center for Environmental Science, MD, USA
12. International Center for Climate and Global Change Research, School of Forestry and Wildlife Sciences, Auburn University, AL, USA
13. Global Carbon Project, CSIRO Oceans and Atmosphere, Canberra, Australia

*Corresponding author

Abstract

Nitrous oxide (N_2O) is the third most important long-lived greenhouse gas and an important stratospheric ozone depleting substance. Agricultural practices and the use of N-fertilizers have greatly enhanced emissions of N_2O. Here we present estimates of N_2O emissions determined from three global atmospheric inversion frameworks during 1998-2016. We find that globally N_2O emissions increased substantially from 2009 and at a faster rate than estimated by the Intergovernmental Panel on Climate Change (IPCC) emission factor (EF) approach. The regions of East Asia and South America made the largest contributions to the global increase. From the inversion-based emissions, we estimate a global EF of $2.3 \pm 0.6\%$, which is significantly larger than the IPCC Tier-1 default for combined direct and indirect emissions of 1.375%. The larger EF and accelerating emission increase found from the inversions suggest that N_2O emission may have a non-linear response at global and regional scales with high levels of N-input.

Main text

Atmospheric N_2O has risen steadily since the mid-20th century[1,2], from approximately 290 ppb in 1940 to 330 ppb in 2017[3,4] - a trend strongly linked to increased reactive nitrogen (Nr) in the environment[5,6]. Nr creation has increased enormously since the mid-20th century largely owing to the Haber-Bosch process (used primarily to produce N-fertilizer), to the cultivation of N-fixing crops, and to the combustion of fossil and bio-fuels[7]. Although increased Nr availability has enabled large increases in food production, it is also associated with a number of environmental problems. Among these is the rise in N_2O emissions: Nr is the substrate of the microbial processes of nitrification and denitrification, both of which produce N_2O as a by-product[8].

N_2O emissions increased from 10-12 TgN y^{-1} prior to the industrial era[5,9] to an average of ~17 TgN/y in the last decade. Agriculture is responsible for the majority of this change, with emissions increasing from 0.3-1.0 TgN y^{-1} in 1850 to 3.9-5.3 TgN y^{-1} in 2010[5,9,10]. To meet

48　　ambitious climate targets, non-CO_2 greenhouse gas emissions will also require reductions[11].
49　　For N_2O, this means reducing agricultural emissions while meeting the growing demand for
50　　food and other agricultural products. This will require changes in human diet and agricultural
51　　practices, and ultimately, improved nitrogen use efficiency (NUE), that is, increasing Nr in
52　　harvest relative to N-input[12,13].

53　　N-input, in particular N-fertilizer use, is one of the best single predictors of N_2O emissions
54　　from agriculture with an estimated emission factor (EF) of ~1% based on emissions measured
55　　from soils[14]. Emission inventories, used for example in reporting under the United
56　　Framework Convention on Climate Change (UNFCCC), are based predominantly on the EF
57　　approach. For direct emissions from agricultural land, the default (Tier-1) value used in
58　　reporting to the UNFCCC is 1% with an uncertainty range from 0.3% to 3% owing to the
59　　variability with agricultural practices, soil properties, and meteorological conditions[14].
60　　Similarly, EFs are used to estimate indirect N_2O emissions from ecosystems downstream and
61　　downwind of agricultural land, which receive Nr via run-off and atmospheric deposition,
62　　amounting to an additional but even more uncertain EF of ~0.375% (Ref 12).

63　　Estimates of the global mean EF have also been made by relating observed changes in
64　　atmospheric N_2O to N-input, the so-called top-down approach, which includes emissions
65　　from agricultural land as well as downstream and downwind ecosystems. Top-down EF
66　　estimates vary from ~2 to 5% and strongly depend on the explanatory variable used,
67　　specifically whether it includes only newly fixed Nr or all Nr sources[5,15,16]. While modelled
68　　N_2O emissions differ depending on the explanatory variable, all EF approaches assume a
69　　linear response of N_2O to N-input. Conversely, evidence from field experiments suggests the
70　　emission response is often nonlinear where N-input is high[17-22]. However, whether this non-
71　　linear response is relevant at large scales and globally is unknown.

72　　N_2O emissions can be estimated regionally independently of EFs using the atmospheric
73　　inversion approach, which utilizes spatiotemporal variations in atmospheric N_2O[23-25]. Here,
74　　we use a global network of N_2O observations to estimate N_2O emissions and their trends
75　　during 1998-2016. These are estimated using three independent inversion frameworks and
76　　transport models (see Supplementary Tables 1&2), providing estimates representing the
77　　systematic uncertainty from errors in modelled transport and stratospheric N_2O loss (see
78　　Methods). Using updated datasets of N-input for the whole agricultural system (i.e. including
79　　crops and grasslands) and of N-surplus for cropping systems (i.e. the difference between N-
80　　input and Nr removed through harvest), we determine the inversion-based emissions
81　　response to these two explanatory variables and examine the linear assumption.

82　　**Emission trends and relation to N-input**

83　　From three inversions, we estimate a global mean emission of 17.0 (16.6-17.4) TgN y^{-1} for
84　　1998 to 2016, with 11.3 (10.2-13.2) TgN y^{-1} from land and 5.7 (3.4-7.2) TgN y^{-1} from ocean
85　　(values in parentheses give the range over three inversions, Supplementary Table 3). The
86　　global emissions presented here are consistent with other top-down estimates ranging
87　　between 15.7 and 18.3 TgN y^{-1} for the year 2000[5,9,23-25]. Similarly, our land emissions
88　　estimate is within the range of other top-down estimates of 11.0 to 12.6 TgN y^{-1}, also for the
89　　year 2000[9,23-25], and the recent estimate from the Nitrogen Model Inter-comparison Project
90　　(NMIP)[10] of 10.0 ± 2.0 TgN y^{-1}.

91　　Top-down methods, including atmospheric inversions, estimate the source as the sum of the
92　　observed change in atmospheric N_2O abundance and the amount lost in the stratosphere. As
93　　the stratospheric loss is not constrained directly by observations this term has considerable
94　　uncertainty, which is propagated into the source estimate. We calculate that stratospheric loss
95　　contributes 1.1 TgN y^{-1} to the discrepancy in the source estimate based on the range of

96   modelled atmospheric lifetimes, 118 to 129 years, and a median abundance of 1522 TgN
97   (Supplementary Table 3) (comparable to previous findings[26]). The discrepancy, however, is
98   larger than the range in source estimates, indicating compensating effects in the inversions.

99   From 2000 the atmospheric growth rate increased steadily from a mean of 0.68 ppb y^{-1} for
100 2000-2005 to 0.98 ppb y^{-1} for 2010-2015, with significant bi- to tri-annual periodicity (Figure
101 1). Before 2000, calibration accuracy and measurement precision were poorer, hence the
102 growth rate for 1998 to 2000 is more uncertain. Our discussion, therefore, focuses on trends
103 from 2000 onwards. Previous studies found a correlation between inter-annual variability in
104 the growth rate and El Niño-Southern Oscillation (ENSO) and attributed it to changes in soil
105 and ocean emissions[27,28]. El Niño is associated with lower growth rates, likely owing to
106 reduced rainfall in tropical and subtropical regions[29] and suppressed upwelling in the eastern
107 tropical Pacific[30]. One study also hypothesized an influence from stratosphere to troposphere
108 transport on inter-annual variability[31]. The increasing trend, however, is likely due to
109 increasing emissions; based on the inversions, emissions increased from 16.3 (15.5-17.1)
110 TgN y^{-1} for 2000-2005 to 17.9 (17.3-18.5) TgN y^{-1} for 2010-2015. This increase is
111 significantly larger than prior estimates, which showed an increase of 0.5 (0.4-0.6) TgN y^{-1}.
112 A change of this magnitude cannot be explained by any known mechanism through the sink,
113 as it would require an increase in atmospheric lifetime of ~20 years, and such a change is
114 unrealistic over this time scale. The atmospheric models used here show no trend in lifetime
115 for this period. The growth in emissions is 90% due to emissions over land (Figure 2)
116 including the land-ocean aquatic continuum and inland water bodies (the spatial resolution
117 of the inversions does not allow these components to be resolved separately).

118 An increase in emissions is consistent with global trends in total N-input and crop N-surplus,
119 which grew by 59 and 18 TgN, respectively, during 2000-2013 (the last year for which data
120 are available) (Figure 3). We include synthetic fertilizer applied to crop and grasslands and
121 total animal excretion, biologically fixed nitrogen in crops and grassland, and NOx
122 deposition from non-agricultural sources (Methods). A similar trend in N-input and N-
123 surplus is seen for China, with increases of 15 and 8 TgN, respectively, as well as for South
124 Asia (i.e., India, Nepal, Bangladesh and Pakistan) and to a lesser extent Brazil. We limit our
125 focus to the global scale and the five countries/regions in Figure 2 because the inversions in
126 other regions are not well constrained due to sparse observations and thus rely on the prior
127 estimates.

128 The regional trends in N-input and N-surplus are consistent with the N_2O emissions derived
129 from the inversions. Emissions were found to increase in China by 0.40 (0.34-0.47) TgN y^{-1}
130 between 2000-2005 and 2010-2015 - significantly larger than prior estimates of 0.23 (0.18-
131 0.32) TgN y^{-1}. Although there is an offset between INV1/INV2 and INV3 for Global land
132 and China, the trends are very similar. The offset is largely due to residual dependence of the
133 posterior on the prior estimates: INV3 used a larger land (and lower ocean) prior compared
134 to INV1/INV2. The uncertainty in all regions was reduced by the inversions (Supplementary
135 Figure 5). The change in South Asia was significantly smaller than in China, 0.14 (0.11-0.16)
136 TgN y^{-1} but larger than prior estimates of 0.03-0.05 TgN y^{-1}. In USA and Europe, emissions
137 were fairly stable over the past nearly two decades. In Brazil, there was an increase between
138 the two periods of 0.26 (0.23-0.29) TgN y^{-1}, but it was small compared to year-to-year
139 emissions variability of 0.22 TgN y^{-1}. The five regions of focus account for ~50% of the
140 global increase between the two time periods, while Africa accounts for ~20%, Central and
141 South America (excluding Brazil) account for ~10%, Southeast Asia and Oceania account
142 for 8%, and 10% was due to changes in ocean emissions (Supplementary Figure 6).

143

Estimation of emission factors

144

145   Using the inversion emission trends and N-input data, we estimated EFs globally and
146   regionally. To calculate EFs, we subtracted estimates of non-soil emissions (i.e., from
147   industry, energy and waste sectors from EDGAR-v4.3.2 (Supplementary Figure 7) and
148   biomass burning from GFED-v4.1s) from the total emissions to give the contribution from
149   soil, which we assume is proportional to N-input. Second, we subtracted the mean of the soil
150   emissions from each inversion over 1998-2016 to remove any offset between inversions.
151   Figure 4 shows scatter plots of N_2O emission anomalies from all inversions versus N-input.
152   The linear regression coefficients provide an estimate of the EF for additional emissions
153   resulting from additional N availability. The EFs were statistically significant ($P < 0.05$)
154   globally, for China, Brazil and South Asia, but not for USA and Europe where changes in N-
155   input and N_2O emission were small compared to scatter in the data (Supplementary Table 4).
156   The emissions are generally higher than proportionate (and more scattered) at the upper range
157   of N-input globally and for China and Brazil, but using non-linear regressions led to only
158   marginal improvements with no difference between quadratic versus exponential functions.
159   Regressions were also calculated relative to N-surplus but no improvement in the correlation
160   or reduction in the residual standard error was found (Supplementary Table 5 and Figure 8).

161   Globally, we find an EF of $2.3 \pm 0.6\%$ for the change in total soil N_2O emission relative to
162   the change in total N-input, including N-fertilizer, manure, biological nitrogen fixation
163   (BNF), and NOx deposition from non-agricultural sources (Figure 5). Our N-input differs
164   slightly from the IPCC 2006 reporting guidelines, which includes (in addition to synthetic
165   fertilizer and manure) Nr from crop residues and mineralization of soil organic matter where
166   soil Nr stocks are changing due to land use or management[14]. On the other hand, our N-input
167   includes total livestock excretion and not only that applied as manure as in the IPCC 2006
168   method. While the IPCC 2006 method does not directly include BNF, it assumes that Nr from
169   BNF is relevant for N_2O production when left on fields in crop residue. We do not have
170   estimates of Nr from mineralization of soil organic matter from land use or management, but
171   this term is likely small compared to other N-inputs. Furthermore, our EF estimates assume
172   that trends in natural emissions of N_2O are negligible over the study period. Since changes
173   in N_2O emissions due to anthropogenic N-input to natural ecosystems is counted as an
174   anthropogenic emission, changes in natural N_2O emissions are primarily related to climatic
175   changes. Natural emissions changed by an estimated 0.7 ± 0.5 TgN y^{-1} since the pre-industrial
176   era and, therefore, likely have negligible impact on our EFs for 2000-2013[10].

177   The IPCC (Tier-1) method gives one EF for direct and another for indirect emissions,
178   whereas we calculate the total EF relative to N-input. To compare the two methods, we
179   estimate the IPCC total EF by adding the equations for direct and indirect emissions (using
180   default parameters) and dividing by total N-input, giving an EF of 1.375% (see Methods).
181   Our global mean EF is higher than the IPCC value but is sensitive to positive emission
182   anomalies in 2010 and 2013 (Figure 2); excluding these values gives an EF that is not
183   statistically different from the IPCC value. A longer time series of inversion-based emissions
184   would help in determining the EF more accurately. However, our estimate of 2.3% agrees
185   well with that of a previous top-down study[5], which found an EF of ~2.5% (Figure 5). Ref 5
186   estimated separate EFs for manure and N-fertilizer, of 2% and 2.5%, respectively, and found
187   this gave a better fit to top-down estimated N_2O emissions throughout the 20th century
188   compared to one EF for total N-input. This was because in the first half of the 20th century
189   Nr in manure was not only derived from contemporaneous N-fixation but was also mined
190   from agricultural soils. Over the past two decades, N-mining from soils occurred only in a
191   few countries, and manure Nr is predominantly derived from fertilizer Nr used to grow crops
192   for livestock feed. Consistent with this, we find for the last nearly two decades that the fit to

193 N$_2$O emissions did not improve if N-fertilizer and manure were considered separately as
194 explanatory variables. A higher EF than the IPCC default, is also plausible considering the
195 evidence of a non-linear response of N$_2$O emission to high levels of N-input[10,17-22], which is
196 discussed below.

197 For China, we find an EF of 2.1 ± 0.4%, which is insensitive to emission anomalies. A high
198 EF for China is credible given the high rates of fertilizer application, low crop NUE (defined
199 as the output/input ratio for cropping systems, Supplementary Figure 9), and possibility of a
200 non-linear response of N$_2$O emission[10,17-22,32,33]. However, our EF for China is associated
201 with systematic uncertainty owing to uncertain trends in non-soil emissions, in particular
202 from industry, which differ substantially between inventories. If the non-soil emission trend
203 is underestimated the EF would be overestimated and vice-versa. For example, using the
204 GAINS inventory estimate for non-soil emissions (instead of EDGAR-v4.32), the EF for
205 China would be only 1.4 ± 0.4% and not distinguishable from the IPCC default. The most
206 important difference between EDGAR and GAINS is the change in emissions from adipic
207 acid production - in EDGAR these are reduced by ~90% between 2005 and 2010 whereas in
208 GAINS they increase by a factor of ~2 (Supplementary Figure 7). The discrepancy arises
209 from assumptions made about adipic acid plants that became operational after 2005,
210 specifically their contribution to total adipic acid production and what emission abatement
211 technologies they use[34,35]. If the GAINS emissions were correct then the increase in
212 emissions from adipic acid production would account for nearly 20% of the total increase in
213 China's emissions since 2005. Trend differences between EDGAR and GAINS have
214 negligible impact on the global EF calculation and for other regions in our study.

215 For Brazil, we calculate an EF of 2.6 ± 0.7%. This value is sensitive to emission anomalies,
216 specifically in 2010 and 2013 (as for the global EF). Removing these anomalies reduces the
217 EF to 2.1 ± 0.7%. Our high EF for Brazil is puzzling due to the relatively high NUE, ~50%,
218 a low portion of synthetic fertilizer in the total N-input, and predominantly low EF values
219 measured at the plot scale (median 0.38%, range 0.13 to 5.14% in cropland)[36]. Several
220 explanations are possible, including insufficient field sampling of soil EFs among the rapidly
221 changing agricultural management systems[37], declining NUE in expanding cereal
222 production[38], underestimated BNF in pastures and sugar cane production[39], effects of ENSO
223 on emissions from Amazon forest soils or from fire[40], varying deforestation trends, as well
224 as growth and intensification of cropland and livestock management[41,42].

225 For South Asia, we find an EF of 0.8 ± 0.4%, which was insensitive to emission anomalies
226 and is lower than the IPCC default. Although South Asia has a low NUE, it uses a smaller
227 portion of synthetic fertilizer in total N-input than China, and has lower intensity of synthetic
228 fertilizer application over crop area, 96 kgN ha^{-1} compared to 281 kgN ha^{-1} in China for the
229 mean over 2000-2013.

230 **Evaluation of the emission factor approach**

231 Globally, the inversion-based soil N$_2$O emissions grew at a faster rate than predicted with the
232 IPCC Tier-1 EF from 2009 (Figure 6). The increase in emissions from 2000-2005 to 2010-
233 2013, of 1.55 (1.44-1.71) TgN y^{-1}, is also more than double that predicted by the IPCC EF,
234 of 0.59 TgN y^{-1}. Using the EF calculated here (2.3%) tended to overestimate the response
235 between 2005-2009 and underestimate it after 2009, when the N-surplus was particularly
236 high. Although a non-linear (quadratic or exponential) function did not markedly improve
237 the residual standard error in the regressions of N$_2$O emission versus N-input (owing to large
238 scatter in the data), there are reasons to think the response may be non-linear, as suggested
239 from field-based studies[17-22]. Mechanisms proposed for a non-linear response with large N-
240 surplus include: 1) more available Nr substrate for nitrification and denitrification[43], 2) high

5

241 soil concentrations of NO_3^- associated with a higher N_2O to N_2 ratio from denitrification[44],
242 3) Nr availability to microorganisms exceeding carbon availability leading to higher rates of
243 N_2O emission[45], and 4) Nr stimulating microbial mobilization of N bound in soil organic
244 matter[46]. We compared the inversion-based soil emissions with the non-linear models in Refs
245 17 and 18 (Supplementary Figure 10) and found that both give slightly higher estimates after
246 2009 compared to the IPCC EF, but still underestimate the emissions.

247 In China, emissions similarly increased at a faster rate than estimated by the IPCC EF after
248 2009. Although the agreement is better in the scenario where the industrial emissions
249 followed the trend in GAINS, if N-input remained at the same high level after 2013, then the
250 IPCC Tier-1 EF would considerably underestimate the emissions also in this scenario from
251 2013. For Brazil, the IPCC EF again underestimates the growth in emissions after 2009, but
252 for South Asia, it reproduces the trend seen in the inversion-based estimates.

253 USA and Europe differ from the other regions in that they have stable and decreasing N-
254 input, respectively. In USA, the nearly flat inversion-based emissions are consistent with EF
255 estimates. The notable negative emission anomaly for 2000-2005, however, is not captured,
256 as it is not due to a change in N-input but rather likely to EF changes driven by meteorological
257 conditions. Precipitation data[47] and the Palmer Drought Severity Index[48] (PDSI) in areas with
258 non-negligible N_2O emissions show persistent dry conditions during 1999-2003, which may
259 have led to a decrease in the EF during that time (Supplementary Figure 11). In the other
260 regions studied, however, there was no clear relationship between N_2O emission anomaly
261 and precipitation, PSDI, or soil temperature. For Europe, the emissions estimated using the
262 EF approach are close to those from the inversions. Although the EF approach shows a small
263 decrease, of 0.01 TgN y^{-1} between 2000-2005 and 2010-2013, no trend is seen in the
264 inversion-based estimate, but it may be that trends related to N-input are still too small to be
265 captured by global scale inversions.

266 **Conclusions and implications**

267 N_2O emissions increased globally by 1.6 (1.4-1.7) TgN y^{-1} between 2000-2005 and 2010-
268 2015, however the rate of increase from 2009 is underestimated using the IPCC Tier-1 default
269 EF. We hypothesize that this is due to an increase in the EF associated with a growing N-
270 surplus. This suggests that the Tier-1 method, which assumes a constant EF, may
271 underestimate emissions when the rate of N-input and the N-surplus are high. This has been
272 demonstrated at field scale, but we show this likely also applies at regional and global scales.
273 We therefore recommend using IPCC Tier-2 approaches and region-specific EFs, especially
274 for high N-input and/or N-surplus conditions, but this would require a body of field
275 measurements to determine accurate values for these EFs. Alternatively, process-based
276 modelling (as used in the IPCC Tier-3 method) validated against observations could help
277 estimate emissions where the N-input and/or N-surplus is high. Our results show that
278 reducing N-surplus (and improving NUE) in high N-input regions should have a more than
279 proportionate outcome in reducing N_2O emissions.

280 **References (main text)**

281 1. Ciais, P. *et al*. Carbon and Other Biogeochemical Cycles. In: *Climate Change 2013:*
282   *The Physical Science Basis. Contribution of Working Group I to the Fifth Assessment*
283   *Report of the Intergovernmental Panel on Climate Change* (2013).
284 2. Ravishankara, A. R., Daniel, J. S. & Portmann, R. W. Nitrous Oxide (N_2O): The
285   Dominant Ozone-Depleting Substance Emitted in the 21st Century. *Science* **326**,
286   123–125 (2009).
287 3. Park, S. *et al*. Trends and seasonal cycles in the isotopic composition of nitrous oxide
288   since 1940. *Nature Geosci* **5**, 261–265 (2012).

6

289   4.   World Meteorological Organisation, *WMO Greenhouse Gas Bulletin* **14**,
290   https://library.wmo.int/doc_num.php?explnum_id=5455 (2018).
291   5.   Davidson, E. A. The contribution of manure and fertilizer nitrogen to atmospheric
292   nitrous oxide since 1860. *Nature Geosci* **2**, 659–662 (2009).
293   6.   Bouwman, A.F. *et al*. Global trends and uncertainties in terrestrial denitrification and
294   N2O emissions. *Philos Trans R Soc B Biol Sci* **368**, 20130112 (2013).
295   7.   Galloway, J. N. *et al*. The Nitrogen Cascade. *BioScience* **53**, 341-356 (2003).
296   8.   Bremner, J. M. Sources of nitrous oxide in soils. *Nutrient Cycling in Agroecosystems*
297   **49**, 7–16 (1997).
298   9.   Syakila, A. & Kroeze, C. The global nitrous oxide budget revisited. *Greenhouse Gas*
299   *Measurement and Management* **1**, 17–26 (2011).
300   10.   Tian, H. *et al*. Global soil N2O emissions since the pre-industrial era estimated by an
301   ensemble of Terrestrial Biosphere Models: Magnitude, attribution and uncertainty.
302   *Global Change Biology*, **25**, 640-659 (2018).
303   11.   Masson-Delmotte, V. *et al*. Summary for Policymakers. In: Global warming of 1.5°C.
304   An IPCC Special Report on the impacts of global warming of 1.5°C above pre-
305   industrial levels and related global greenhouse gas emission pathways, in the context
306   of strengthening the global response to the threat of climate change, sustainable
307   development, and efforts to eradicate poverty, *World Meteorological Organization*
308   (2018).
309   12.   Davidson, E. A., Suddick, E. C., Rice, C. W. & Prokopy, L. S. More Food, Low
310   Pollution (Mo Fo Lo Po): A Grand Challenge for the 21st Century. *Journal of*
311   *Environment Quality* **44**, 305–7 (2015).
312   13.   Springmann, M. *et al*. Options for keeping the food system within environmental
313   limits. *Nature* **562**, 519-525 (2018).
314   14.   De Klein, C. *et al*. in IPCC Guidelines for National Greenhouse Gas Inventories,
315   Prepared by the National Greenhouse Gas Inventories Programme 4, 1–54 (2006).
316   15.   Crutzen, P. J., Mosier, A. R., Smith, K. A. & Winiwarter, W. N2O release from agro-
317   biofuel production negates global warming reduction by replacing fossil fuels. *Atmos*
318   *Chem Phys* **8**, 389–395 (2008).
319   16.   Smith, K. A., Mosier, A. R., Crutzen, P. J. & Winiwarter, W. The role of N2O derived
320   from crop-based biofuels, and from agriculture in general, in Earth's climate. *Philos*
321   *Trans Royal Soc B Biol Sci* **367**, 1169–1174 (2012).
322   17.   Shcherbak, I., Millar, N. & Robertson, G. P. Global meta-analysis of the nonlinear
323   response of soil nitrous oxide (N2O) emissions to fertilizer nitrogen. *Proc Natl Acad*
324   *Sci USA* **111**, 9199–9204 (2014).
325   18.   Hoben, J. P. *et al*. Nonlinear nitrous oxide (N2O) response to nitrogen fertilizer in on-
326   farm corn crops of the US Midwest. *Global Change Biology* **17**(2), 1140–1152,
327   (2010).
328   19.   Signor, D., Cerri, C. E. P., & Conant, R. N2O emissions due to nitrogen fertilizer
329   applications in two regions of sugarcane cultivation in Brazil. *Environ Res Lett*, **8**(1),
330   015013 (2013).
331   20.   Song, X., Liu, M., Ju, X., Gao, B., Su, F., Chen, X., & Rees, R. M. Nitrous Oxide
332   Emissions Increase Exponentially When Optimum Nitrogen Fertilizer Rates Are
333   Exceeded in the North China Plain. *Environmental Science & Technology*, **52**(21),
334   12504–12513 (2018).
335   21.   Philibert, A., Loyce, C., & Makowski, D. Quantifying Uncertainties in N2O Emission
336   Due to N Fertilizer Application in Cultivated Areas. *PLoS One*, **7**(11), e50950 (2012).
337   22.   Gerber, J. S., Carlson, K. M., Makowski, D., Mueller, N. D., Garcia de Cortazar-
338   Atauri, I., Havlik, P., *et al*. Spatially explicit estimates of N2O emissions from

339   croplands suggest climate mitigation opportunities from improved fertilizer
340   management. *Glob. Change Biol.*, **22**(10), 3383–3394 (2016).

341 23. Saikawa, E. *et al*. Global and regional emissions estimates for N_2O. *Atmos Chem*
342   *Phys* 14, 4617–4641 (2014).

343 24. Hirsch, A. I. *et al*. Inverse modeling estimates of the global nitrous oxide surface flux
344   from 1998–2001. *Global Biogeochem. Cycles*, **20**, GB1008,
345   doi:10.1029/2004gb002443 (2006).

346 25. Huang, J. *et al*. Estimation of regional emissions of nitrous oxide from 1997 to 2005
347   using multinetwork measurements, a chemical transport model, and an inverse
348   method. *J. Geophys. Res.*, **113**, D17313, doi:10.1029/2007JD009381 (2008).

349 26. Prather, M. J. *et al*. Measuring and modeling the lifetime of Nitrous Oxide including
350   its variability. *J. Geophys. Res. Atmos*. **120**, 5693-5705 (2015).

351 27. Thompson, R. L. *et al*. Interannual variability in tropospheric nitrous oxide. *Geophys.*
352   *Res. Lett*. **40**, 4426–4431 (2013).

353 28. Ishijima, K., Nakazawa, T. & Aoki, S. Variations of atmospheric nitrous oxide
354   concentration in the northern and western Pacific. *Tellus B* **61**, 408–415 (2009).

355 29. Werner, C., Butterbach-Bahl, K., Haas, E., Hickler, T., & Kiese, R. A global
356   inventory of N_2O emissions from tropical rainforest soils using a detailed
357   biogeochemical model. *Global Biogeochem. Cycles*, **21**, GB3010 (2007).

358 30. Nevison, C. D., Mahowald, N. M., Weiss, R. F., & Prinn, R. G. Interannual and
359   seasonal variability in atmospheric N_2O. *Global Biogeochem. Cycles*, **21**, GB3017
360   (2007).

361 31. Nevison, C. D. *et al*. Exploring causes of interannual variability in the seasonal cycles
362   of tropospheric nitrous oxide. *Atmos. Chem. Phys*. **11**, 3713–3730 (2011).

363 32. Lassaletta, L. *et al*. 50 year trends in nitrogen use efficiency of world cropping
364   systems: the relationship between yield and nitrogen input to cropland. *Environ. Res.*
365   *Lett.* **9**, 105011 (2014).

366 33. Zhang, X. *et al*. Managing nitrogen for sustainable development. *Nature* **528**, 51-59
367   (2015).

368 34. Winiwarter, W. *et al*. Technical opportunities to reduce global anthropogenic
369   emissions of nitrous oxide. *Environ Res Lett*, **13**(1), 014011 (2018).

370 35. Schneider, L., Lazarus, M., & Kollmuss, A. Industrial N_2O Projects Under the CDM:
371   Adipic Acid - A Case of Carbon Leakage? Stockholm Environment Institute Working
372   Paper WP-US-1006 (2010).

373 36. Meurer, K. H. E. *et al*. Direct nitrous oxide (N_2O) fluxes from soils under different
374   land use in Brazil - a critical review. *Environ Res Lett* **11**(2), 023001 (2016).

375 37. Jankowski, K., C. *et al*. Deep soils modify environmental consequences of increased
376   nitrogen fertilizer use in intensifying Amazon agriculture. *Scientific Reports*, **8**:13478
377   (2018).

378 38. Pires, M. V., da Cuhna, D. A., de Matos Carlos, S., & Heil Costa, M. Nitrogen-Use
379   Efficiency, Nitrous Oxide Emissions, and Cereal Production in Brazil: Current
380   Trends and Forecasts. *PLoS One*, **10**(8), 1–20 (2015).
381   http://doi.org/10.1371/journal.pone.0135234

382 39. Herridge, D. F., Peoples, M. B., & Boddey, R. M. Global inputs of biological
383   nitrogen fixation in agricultural systems. *Plant and Soil*, **311**(1-2), 1–18 (2008).

384 40. Davidson, E. A. *et al*. The Amazon basin in transition. *Nature*, **481**(7381), 321–328
385   (2012).

386 41. Zalles, V., *et al*. Near doubling of Brazil's intensive row crop area since 2000. *Proc*
387   *Natl Acad Sci*. **22**, doi:10.1073/pnas.1810301115 (2018).

388 42. Merry, F., & Soares-Filho, B. Will intensification of beef production deliver
389   conservation outcomes in the Brazilian Amazon? *Elem Sci Anth*, **5**, 24 (2017).
390 43. Van Groenigen, J. W. *et al*. Towards an agronomic assessment of N_2O emissions: a
391   case study for arable crops. *European Journal of Soil Science*, **61**(6), 903–913 (2010).
392 44. Firestone, M. K. Biological Denitrification. In: *Nitrogen in Agricultural Soils,*
393   *Agronomy Monograph* **22**, 289–326 (1982).
394 45. Firestone, M. K., & Davidson, E. A. Microbiological basis of NO and N_2O
395   production and consumption in soil. In: *Exchange of Trace Gases Between*
396   *Terrestrial Ecosystems and the Atmosphere*, M. O. Andreae & D. S. Schimel (Eds.),
397   7–21 (1989).
398 46. Kim, D.-G., Hernandez-Ramirez, G., & Giltrap, D. Linear and nonlinear dependency
399   of direct nitrous oxide emissions on fertilizer nitrogen input: A meta-analysis.
400   *Agriculture Ecosystems & Environment*, **168**, 53–65 (2013).
401 47. Adler, R. F. *et al*. The Version-2 Global Precipitation Climatology Project (GPCP)
402   Monthly Precipitation Analysis (1979–Present). *J. Hydrometeor*, **4**(6), 1147–1167
403   (2003)
404 48. Dai, A. Characteristics and trends in various forms of the Palmer Drought Severity
405   Index during 1900–2008. *J. Geophys. Res*. **116**(D12) (2011).

406 **Methods**

407 Emissions were estimated using three independent atmospheric inversion frameworks (see
408 Supplementary Table 1). The frameworks all used the Bayesian inversion method, which
409 finds the optimal emissions, that is, those, which when coupled to a model of atmospheric
410 transport, provide the best agreement to observed N_2O mixing ratios while remaining with
411 the uncertainty limits of the prior estimates. In other words, the emissions that minimize the
412 cost function:

413 $$J(\mathbf{x}) = \frac{1}{2}(\mathbf{x} - \mathbf{x_b})^T \mathbf{B}^{-1}(\mathbf{x} - \mathbf{x_b}) + \frac{1}{2}(\mathbf{y} - H(\mathbf{x}))^T \mathbf{R}^{-1}(\mathbf{y} - H(\mathbf{x})) \qquad (1)$$

414 where $\mathbf{x}$ and $\mathbf{x_b}$ are, respectively, vectors of the optimal and prior emissions, $\mathbf{B}$ is the prior
415 error covariance matrix, $\mathbf{y}$ is a vector of observed N_2O mixing ratios, $\mathbf{R}$ is the observation
416 error covariance matrix, and $H(\mathbf{x})$ is the model of atmospheric transport (for details on the
417 inversion method see Ref. 49). The optimal emissions, $\mathbf{x}$, were found by solving the first
418 order derivative of equation (1):

419 $$J'(\mathbf{x}) = \mathbf{B}^{-1}(\mathbf{x} - \mathbf{x_b}) + (H'(\mathbf{x}))^T \mathbf{R}^{-1}(\mathbf{y} - H(\mathbf{x})) = 0 \qquad (2)$$

420 where $(H'(\mathbf{x}))^T$ is the adjoint model of transport. In frameworks INV1 and INV2, equation
421 (2) was solved using the variational approach[50,51], which uses a descent algorithm and
422 computations involving the forward and adjoint models[52]. In framework INV3, equation (2)
423 was solved directly by computing a transport operator, $\mathbf{H}$ from integrations of the forward
424 model, such that $\mathbf{Hx}$ is equivalent to $H(\mathbf{x})$, and taking the transpose of $\mathbf{H}$[53].

425 Each of the inversion frameworks used a different model of atmospheric transport with
426 different horizontal and vertical resolutions (see Supplementary Table 1). The transport
427 models TOMCAT and LMDz, used in INV1 and INV2 respectively, were driven by ECMWF
428 ERA-Interim wind fields, and the model, MIROC4-ACTM, used in INV3, was driven by
429 JRA-55 wind fields. While INV1 and INV2 optimized the emissions at the spatial resolution
430 of the transport model, INV3 optimized the error in the emissions aggregated into 84 land
431 and ocean regions[53]. All frameworks optimized the emissions with monthly temporal
432 resolution. The transport models included an online calculation of the loss of N_2O in the

9

433 stratosphere due to photolysis and oxidation by $O(^1D)$ resulting in mean atmospheric
434 lifetimes of between 118 and 129 years, broadly consistent with recent independent estimates
435 of the lifetime of 116 ± 9 years[26].

436 The inversions used N_2O measurements of discrete air samples from the National Oceanic
437 and Atmospheric Administration Carbon Cycle Cooperative Global Air Sampling Network
438 (NOAA) and the Commonwealth Scientific and Industrial Research Organisation network
439 (CSIRO). In addition, we used measurements from in-situ instruments in the Advanced
440 Global Atmospheric Gases Experiment network (AGAGE), the NOAA CATS network, and
441 from individual sites operated by University of Edinburgh (UE), National Institute for
442 Environmental Studies (NIES) and the Finish Meteorological Institute (FMI) (see
443 Supplementary Figure 1). Measurements from networks other than NOAA were corrected to
444 the NOAA calibration scale, NOAA-2006A[54], using the results of the WMO Round Robin
445 inter-comparison experiment (https://www.esrl.noaa.gov/gmd/ccgg/wmorr/). Frameworks
446 INV1 and INV2 used a total of 83 discrete air sampling sites, 15 in-situ sampling sites and
447 discrete air samples from the NOAA network of ships and moorings, and INV3 used 37
448 discrete air sampling sites. Daily average observations were assimilated in INV1 and INV3,
449 while INV2 assimilated hourly afternoon values for low altitude sites and nighttime values
450 for mountain sites to minimize errors in the modeled mixing ratios from errors in the modeled
451 planetary boundary layer heights and local mountain-valley circulation.

452 Each framework applied its own method for calculating the uncertainty in the observation
453 space, the square of which gives the diagonal elements of the observation error covariance
454 matrix **R**. The observation space uncertainty accounts for measurement and model
455 representation errors and is equal to the quadratic sum of these terms. INV1 assumed a
456 measurement uncertainty of 0.4 ppb and, in addition, estimated the model representation error
457 as the mixing ratio gradient across the grid cell in which the observation is located and the
458 surrounding ones, resulting in a mean total uncertainty of 0.48 ppb. INV2 assumed a
459 measurement uncertainty of 0.3 ppb and estimated the representation error in the same way
460 as INV1, resulting in a mean total uncertainty of 0.50 ppb. INV3 used a measurement
461 uncertainty of 0.32 ppb and estimated the representation error as 1-sigma standard deviation
462 of daily observations at each site.

463 Prior emissions were used in all frameworks and were based on existing estimates from
464 terrestrial biosphere and ocean biogeochemistry models as well as from inventories (see
465 Supplementary Table 2). INV1 and INV2 used the same prior estimates for emissions from
466 natural and agricultural soils from the model OCN-v1.1, for ocean emissions from the model
467 PlankTOM5, and for biomass burning emissions from the Global Fire Emissions Database
468 (GFED-v4.1s). OCN parameterizes N_2O emissions from nitrification and denitrification in
469 soils and accounts for N-input from N-fertilizer, manure, atmospheric deposition, and
470 biological nitrogen fixation. The model is driven by CRU-NCEP meteorological data and
471 uses inter-annually varying N-input[55]. PlankTOM5 uses the observed correlation between
472 apparent oxygen utilisation and excess N_2O in oxic waters to estimate the open ocean source
473 of N_2O production and the increased yield of N_2O in suboxic waters from both nitrification
474 and denitrification as an additional source in oxygen minimum zones[56]. The model,
475 PlankTOM5, is incorporated into the ocean general circulation model, NEMO v3.1, which is
476 forced with NCEP meteorology. For non-soil anthropogenic emissions (namely those from
477 energy, industry and waste sectors), both INV1 and INV2 use the Emission Database for
478 Greenhouse Gas Research (EDGAR) but differing versions (see Supplementary Table 2).
479 INV3 used GEIA (Global Emissions Initiative) for emissions from natural soils and ocean
480 emissions from Manizza et al. 2012[57]. Manizza et al. model ocean emission using the
481 correlation of apparent oxygen utilization and excess N_2O in oxic waters and their model is

482　incorporated into the MIT General Circulation Model. For soil and non-soil anthropogenic
483　emissions, INV3 used a third version of EDGAR (see Supplementary Table 2), which also
484　includes agricultural burning but they did not specifically account for wildfire emissions in
485　the prior estimates.

486　Prior uncertainties were estimated in all the inversion frameworks for each grid cell (INV1
487　and INV2) or for each region (INV3) and square of the uncertainties formed the diagonal
488　elements of the prior error covariance matrix **B**. INV1 and INV2 estimated the uncertainty
489　as proportional to the prior value in each grid cell, and INV2 set lower and upper limits for
490　the uncertainty of 3×10^{-9} and 5×10^{-8} kgN m^{-2} h^{-1}, respectively. INV3, on the other hand, set
491　the uncertainty uniformly for the land regions at 1 TgN y^{-1} and for the ocean regions at 0.5
492　TgN y^{-1}. INV2 was the only framework to account for spatial and temporal correlations in
493　the errors (resulting in off-diagonal elements in the prior error covariance matrix) using an
494　exponential decay model with distance and time with correlation scale lengths of 500 km
495　over land and 1000 km over ocean and 90 days.

496　The optimized emissions were interpolated to 1°×1° (see Supplementary Figure 2) and the
497　regional emissions were calculated by integrating the gridded emissions within each region
498　or country. For each region, estimates of the non-soil anthropogenic emissions (i.e., from
499　industry, energy and waste sectors) from EDGAR-v4.32 and the biomass burning emissions
500　from GFED-v4.1s were subtracted from the total emissions from the inversions to give only
501　the contribution from soil, which is assumed to be proportional to N-input. This assumes that
502　the error in the estimate for non-soil anthropogenic emissions is substantially smaller than
503　that in the soil emissions (Supplementary Figure 7).

504　The inversions were validated by integrating the forward models with the posterior emissions
505　and comparing the simulated mixing ratios with independent observations, i.e., observations
506　that were not assimilated in the inversions. We compared with CONTRAIL (Comprehensive
507　Observation　Network　for　TRace　gases　by　AirLiner,　http://www.jal-
508　foundation.or.jp/shintaikikansokue/contrail_index.htm), which has N$_2$O observations at
509　regular intervals across the Pacific since 2005 (Supplementary Figure 3). All three inversions
510　showed a similar level of performance with differences typically of <0.5 ppb. We also
511　compared with aircraft profile measurements over USA from NOAA from sites with data for
512　the early 2000s (Supplementary Figure 4). We found that INV1 tended to underestimate N$_2$O
513　in the lower troposphere over the contiguous USA for the early 2000s, hence we did not
514　include the emissions data for USA prior to 2005 in our analyses.

515　We calculated N inputs to the whole agricultural system including crops and grasslands. Total
516　inputs correspond to synthetic fertilizer application, animal excretion (even if finally not
517　reaching crops or grasslands), biological nitrogen fixation, and NOx deposition on
518　agricultural land. Total outputs correspond to crop and animal production. Total surplus is
519　calculated as the difference between inputs and outputs. In this budget, we neglected the
520　small part of crop production that is locally consumed by livestock. Synthetic fertilizer
521　application is based on the FAOSTAT dataset (http://www.fao.org/home/en/) with several
522　inputs from the International Fertilizer Association (https://www.fertilizer.org/). Total
523　animal excretion is calculated using the FAOSTAT livestock inventory and dynamic
524　excretion factors, biological N fixation is calculated from crop productivities[58] and
525　atmospheric deposition was from Ref 59. Grassland nitrogen fixation was based on the
526　grassland production estimated following Ref 60 and validated through comparison with the
527　IMAGE model[61]. We consider 20% of grass species to be N fixing legumes and that their N
528　fixation is equal to 1.4 times the N from aerial production to also account for below ground
529　biomass production, which would otherwise not be included[58]. N output in harvested crops
530　is based on crop productivity and N content of 177 crops, utilizing data from the FAOSTAT

11

531 database. See also the detailed methodology in Refs 32 and 60. We consider the N-surplus
532 and NUE of cropping systems, as they are widely used as an indicator of the agronomic and
533 environmental performance of agricultural systems.

534 Emission factors were determined by a linear regression of N_2O soil emission versus total N-
535 input. The total N-input consisted of sources of N from synthetic fertilizer (N_{SF}), organic
536 fertilizer and manure (N_{ON}), biological nitrogen fixation (N_{BNF}) and NOx deposition from
537 non-agricultural sources. This emission factor represents the total of direct and indirect
538 emissions. The emission factors calculated in this study were compared to the IPCC Tier-1
539 default values, where the total IPCC EF was calculated by taking the weighted average of the
540 direct (EF_{dir}) and indirect factors for deposition (EF_{dep}) and leaching (EF_{leach}) according to:

541
$$EF_{tot} = EF_{dir} + EF_{dep}\left(f_{SF}\frac{N_{SF}}{N_{tot}} + f_{ON}\frac{N_{ON}}{N_{tot}} \right) + EF_{leach}f_{leach} \tag{3}$$

542 where f_{SF} and f_{ON} are the fractions of synthetic and organic fertilizer volatized, respectively,
543 and f_{leach} is the fraction of N lost by leaching and runoff [12]. The modelled N_2O emission
544 (F_{N2O}) using the IPCC emission factors was calculated as:

545
$$F_{N_2O} = EF_{dir}\left(N_{SF} + N_{ON} + N_{BNF} \right) + EF_{dep}\left(N_{SF}f_{SF} + N_{ON}f_{ON} \right) +$$
$$EF_{leach}\left(N_{SF} + N_{ON} + N_{BNF} \right)f_{leach} \tag{4}$$

546 using the N-input dataset described above.

547 **References (Methods)**

548 49. Tarantola, A. *Inverse problem theory and methods for model parameter estimation*.
549   Society for Industrial and Applied Mathematics (2005).
550 50. Thompson, R. L. *et al*. Nitrous oxide emissions 1999 to 2009 from a global
551   atmospheric inversion. *Atmos. Chem. Phys*. **14**, 1801–1817 (2014).
552 51. Wilson, C., Chipperfield, M. P., Gloor, M., & Chevallier, F. Development of a
553   variational flux inversion system (INVICAT v1.0) using the TOMCAT chemical
554   transport model. *Geosci Model Dev* **7(**5), 2485–2500 (2014).
555 52. Fisher, M. & Courtier, P. Estimating the covariances matrices of analysis and forecast
556   error in variational data assimilation. *Technical Memorandum of the European
557   Centre for Medium-Range Weather Forecasts* **220**, 1-26 (1995).
558 53. Patra, P. K. *et al*. Improved Chemical Tracer Simulation by MIROC4.0-based
559   Atmospheric Chemistry-Transport Model (MIROC4-ACTM). *SOLA* **14**, 91–96
560   (2018).
561 54. Hall, B. D., Sutton, G. S. & Elkins, J. W. The NOAA nitrous oxide standard scale for
562   atmospheric observations. *J Geophys Res* **112**, D09305 (2007).
563 55. Zaehle, S., Ciais, P., Friend, A. D. & Prieur, V. Carbon benefits of anthropogenic
564   reactive nitrogen offset by nitrous oxide emissions. *Nature Geosci* **4**, 601–605 (2011).
565 56. Suntharalingam, P. *et al*. Quantifying the impact of anthropogenic nitrogen
566   deposition on oceanic nitrous oxide. *Geophys. Res. Lett*. **39**, L07605 (2012).
567 57. Manizza, M., Keeling, R. F. & Nevison, C. D. On the processes controlling the
568   seasonal cycles of the air–sea fluxes of O_2 and N_2O: A modelling study. *Tellus B:
569   Chemical and Physical Meteorology* **64**, 18429 (2012).
570 58. Anglade, J., Billen, G., & Garnier, J., Relationships for estimating N_2 fixation in
571   legumes: incidence for N balance of legume-based cropping systems in Europe.
572   *Ecosphere* **6**, 37 (2015).
573 59. Dentener, F. *et al*. Nitrogen and sulfur deposition on regional and global scales: A
574   multimodel evaluation. *Global Biogeochem. Cycles*, **20**(4) (2006).

575 60. Lassaletta, L. *et al*. Nitrogen use in the global food system: Past trends and future
576   trajectories of agronomic performance, pollution, trade, and dietary demand. *Environ.*
577   *Res. Lett.* **11**. (2016).
578 61. Stehfest, E. *et al*. Integrated Assessment of Global Environmental Change with
579   IMAGE 3.0. Model Description and Policy Applications. Netherlands Environmental
580   Assessment Agency, The Hague (2014).
581 62. Le Noë, J., Billen, G., & Garnier, J. How the structure of agro-food systems shapes
582   nitrogen, phosphorus, and carbon fluxes: The generalized representation of agro-food
583   system applied at the regional scale in France. *Science of the Total Environment*, **586**,
584   42–55 (2017).

585 **Corresponding Author**

586 Correspondence and requests for materials should be addressed to RLT.

587 **Acknowledgements**

612 **Author contributions**

613 RLT designed the study, contributed inversion results and prepared the manuscript; LL
614 prepared the N-data and contributed to the manuscript; PKP, CW and MPC contributed
615 inversion results and to the manuscript; KCW, AG, ENK, WW and EAD helped with the
616 analysis and contributed to the manuscript; HT and JCG contributed to the manuscript.

617 **Competing interests statement**

618 The authors declare that they have no competing interests.

619 **Data availability**

620 Atmospheric observations used in the inversions are available from the databases indicated
621 in the Acknowledgements. The CONTRAIL data used in the validation of the inversion
622 results are available on request to H. Matsueda (MRI-JMA). The inversion output data are
623 available from http://doi.org/10.5281/zenodo.3384591 and the N-data are available from
624 https://doi.org/10.5281/zenodo.3384678. The inversion codes are available from the
625 following authors on reasonable request: C. Wilson (c.wilson@leeds.ac.uk) for INV1; R.
626 Thompson (rlt@nilu.no) for INV2; and P. Patra (prabir@jamstec.go.jp) for INV3.

627

Figure 1. Observed and modelled global mean growth rates of N_2O. Observed growth rates are shown based on the NOAA discrete sampling network and, for comparison, the AGAGE network. Modelled growth rates were calculated by sampling 4D mixing ratio fields at the times and locations of the NOAA observations. All growth rates were calculated with annual time steps and are shown as 1-year running averages.
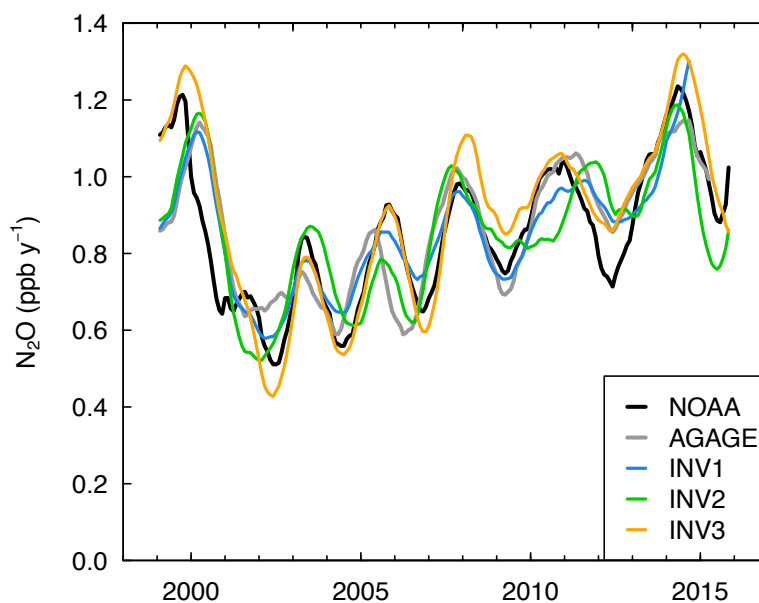

Figure 2. Annual N_2O emissions from the atmospheric inversions for 1998 to 2016 (units TgN y^{-1}). Dashed lines show the prior and solid lines the posterior emissions. INV1 data prior to 2005 for USA are shown as a dotted line as these data are more uncertain (see Methods).
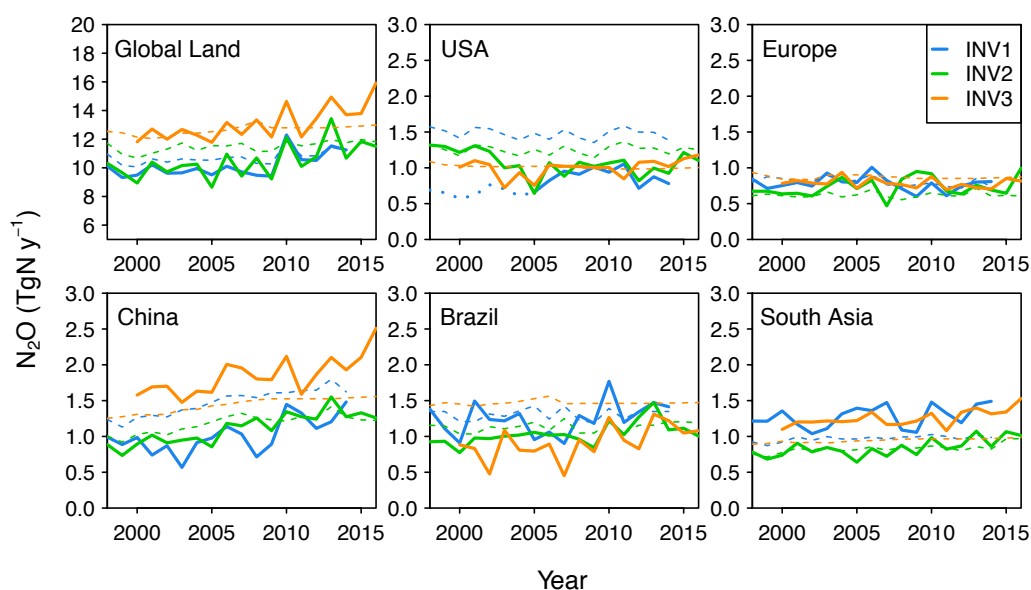
Figure 3. N-inputs to world crops and grasslands (units TgN y^{-1}) and N-surplus in the cropping systems. (N-fert is synthetic fertilizer, N-fixed is biologically fixed N, NOx-dep is NOx deposition, N-surplus is surplus only for cropping systems).
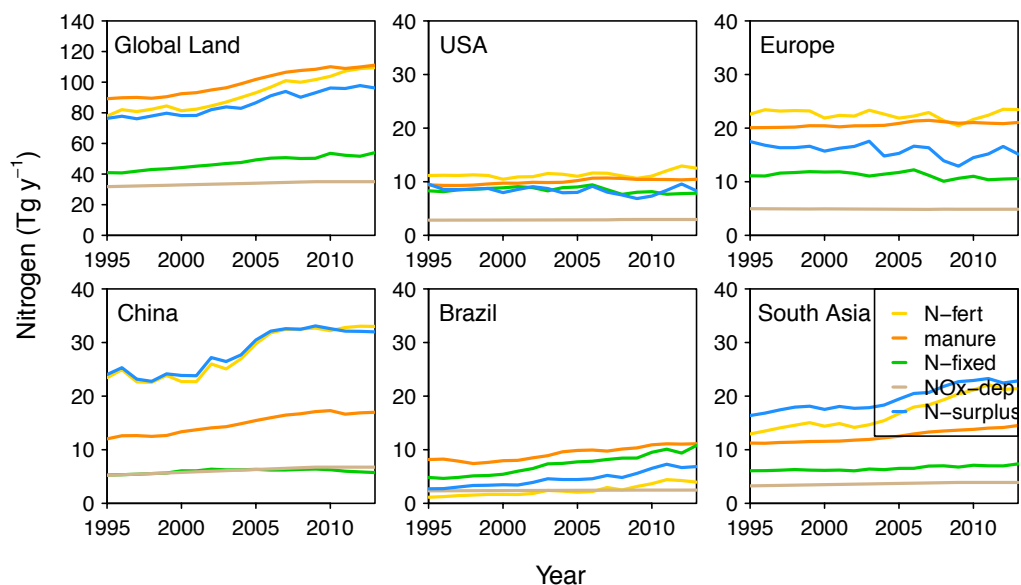

Figure 4. Scatter plots of the N$_2$O emission anomalies versus N-input (units TgN y^{-1}). The emissions were corrected for the non-soil component and the anomalies were calculated relative to the mean for 1998 to 2013. The symbols are colour-coded by year (circles = INV1, squares = INV2, diamonds = INV3). The solid line shows the regression and the dotted lines the confidence range. In the case that the regression is not significant ($P > 0.05$) a dashed line is used for the regression. (INV1 was excluded for USA owing to the poorer model-observation comparison for 1998-2005).
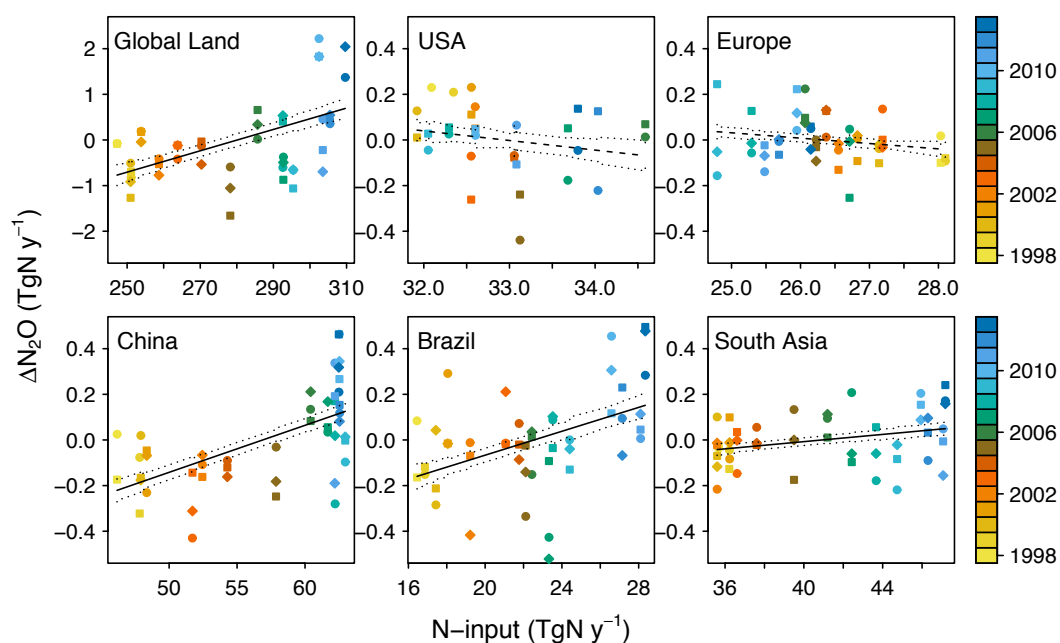

16

Figure 5. Comparison of emission factors (EF) from this study and from recent literature. The white to red circles are the EFs calculated over all inversions in this study and the colour indicates the correlation coefficient (see legend). The grey points are the EFs calculated from the individual inversions where the correlation was significant (circles = INV1, squares = INV2, diamonds = INV3). A second EF is shown (red diamond) for China using the GAINS estimate for the non-soil anthropogenic emissions. For the values reported by this study, the error bars show the standard error and for the other studies, they show the reported uncertainty.
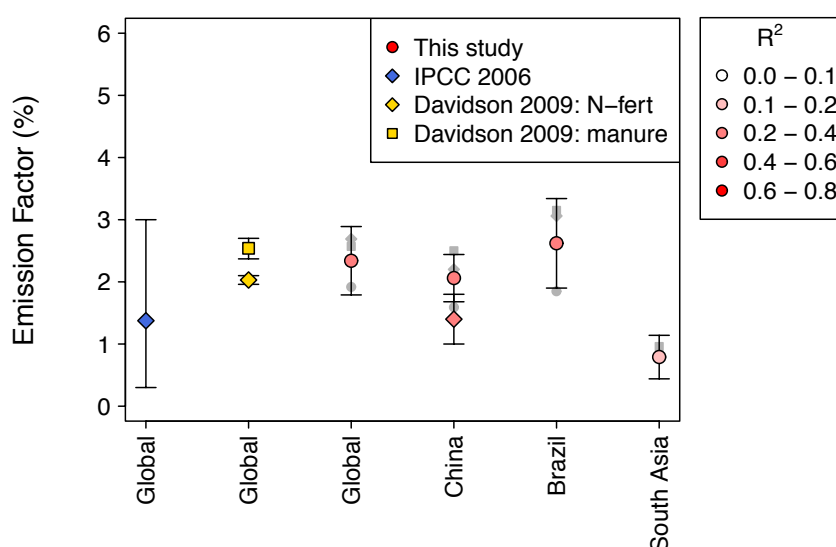

Figure 6. Comparison of N_2O emissions from the inversions (corrected for the non-soil component) with those calculated using the EF approach (units TgN y^{-1}). The inversion results are shown as the mean (black line) and range (grey shading). A scalar value was added to the emissions time series' so that they matched the inversion mean in the year 2000. The EF results are shown using the IPCC value (blue) and the linear fit from this study (green). For USA and Europe the regional EFs from this study were not significant so the global EF from this study was used instead. For China, the emissions corrected using GAINS for the non-soil component (instead of EDGAR-v4.32) are also shown (black dotted line).